Pergamon

Geochimica et Cosmochimica Acta, Vol. 67, No. 11, pp. 2077–2091, 2003

0016-7037/03 $30.00 + .00

doi:10.1016/S0016-7037(02)01272-3

Core formation in the Earth and Moon: New experimental constraints from V, Cr, and Mn

NANCY L. CHABOT[1,*] and CARL B. AGEE[2,1]

[1]Department of Geological Sciences, 112 A. W. Smith Bldg., Case Western Reserve University, Cleveland, OH 44106-7216, USA
[2]Mail Code SA, NASA Johnson Space Center, Houston, TX 77058, USA

(*Received May* 24, 2002; *accepted in revised form October* 2, 2002)

Abstract—The mantles of the Earth and Moon are similarly depleted in V, Cr, and Mn relative to the concentrations of these elements in chondritic meteorites. The similar depletions have been used as evidence that the Moon inherited its mantle from the Earth after a giant impact event. We have conducted liquid metal–liquid silicate partitioning experiments for V, Cr, and Mn from 3 to 14 GPa and 1723 to 2573 K to understand the behavior of these elements during planetary core formation. Our experiments have included systematic studies of the effects of temperature, silicate composition, metallic S-content, metallic C-content, and pressure. Temperature has a significant effect on the partitioning of V, Cr, Mn, with all three elements increasing their partitioning into the metallic liquid with increasing temperature. In contrast, pressure is not observed to affect the partitioning behavior. The experimental results show the partitioning of Cr and Mn are hardly dependent on the silicate composition, whereas V partitions more strongly into depolymerized silicate melts. The addition of either S or C to the metallic liquid causes increased metal–silicate partition coefficients for all three elements. Parameterizing and applying the experimental data, we find that the Earth's mantle depletions of V, Cr, and possibly Mn can be explained by core formation in a high-temperature magma ocean under oxygen fugacity conditions about two log units below the iron–wüstite buffer, though the depletion of Mn may be due entirely to its volatility. However, more oxidizing conditions proposed in recent core formation models for the Earth cannot account for any of the depletions. Additionally, because we observe no pressure effect on the partitioning behavior, the data do not require the mantle of the Moon to be derived from the Earth's mantle, although this is not ruled out. All that is required to create depletions of V, Cr, and Mn in a mantle is a planetary body that is hot enough and reducing enough during its core formation. Such conditions could have existed on the Moon-forming impactor.

1. INTRODUCTION

Ringwood (1966) was the first to note that V, Cr, and Mn are depleted in the Earth's mantle relative to CI chondrites. He proposed that during early differentiation, these elements were preferentially extracted from the mantle and partitioned into the Earth's core in highly reduced form. Dreibus and Wänke (1979) recognized that the Moon is similarly depleted in V, Cr, and Mn and suggested that this similarity was evidence of a common genesis for the Earth and Moon. Subsequent studies proposed that the Moon inherited its mantle, and the V, Cr, and Mn depletions, from the Earth during the impact-induced formation of the Moon (Ringwood, 1986; Wänke and Dreibus, 1986).

The abundances of V, Cr, and Mn in the silicate portions of the Earth and the Moon are slightly depleted relative to CI chondritic values. However, V, Cr, and Mn, which usually exhibit lithophile (rock-loving) tendencies, are not depleted at the levels of the moderately or highly siderophile (metal-loving) elements, which are depleted by orders of magnitude in the Earth's mantle relative to CI chondrites. Consequently, the estimated depletions of V, Cr, and Mn in the Earth and the Moon are more sensitive to the choice of chondrite group used to represent the undepleted composition than are the estimated depletions of the more siderophile elements.

Elements can also be depleted in the Earth and Moon relative to chondritic values due to their volatility. This is not a factor for V, which is refractory, but for Cr and especially for Mn, depletions due to volatility must be considered. The review of Walter et al. (2000) recently estimated the depletions of V, Cr, and Mn in the silicate portions of the Earth and Moon. After taking into account uncertainties in the depletion estimates due to variations among chondrite groups, the volatility of Cr and Mn, and the measured mantle abundances, Walter et al. (2000) concluded that V, Cr, and Mn were all slightly depleted in the silicate Earth and Moon by a process such as core formation. McDonough (1999) also proposed significant amounts of V and Cr in the Earth's core and calculated that if there was no V in the Earth's core, the bulk Earth Mg/V ratio would be greater than that observed in all chondritic meteorites. In contrast to the estimate of Walter et al. (2000), O'Neill and Palme (1998) pointed out that the Mn/Na ratio in the Earth's mantle is the same as that of all types of chondrites, with the exception of the more reduced enstatite chondrites. They suggested the chondritic Mn/Na ratio indicates that the depletion of Mn in the Earth's mantle can be explained by volatility alone, without requiring significant partitioning of Mn into the Earth's core. The possibility of lower mantle minerals, such as magnesiowüstite, playing a role in the observed depletions of V, Cr, and Mn has also been suggested (Righter, 2003).

Previous experiments have been conducted to explore what influence the formation of Earth's metallic core would have on

* Author to whom correspondence should be addressed (nlc9@po.cwru.edu).
[1] Present address: Institute of Meteoritics, Department of Earth and Planetary Sciences, University of New Mexico, Albuquerque, NM 87131

the V, Cr, and Mn abundances in the mantle. At low pressure and temperature, V, Cr, and Mn were not found to be sufficiently siderophile to be depleted by core formation and to account for the observed mantle abundances (Drake et al., 1989). Ringwood et al. (1990) performed experiments between solid iron and Fe-O melts at 16 GPa and 1973 K and reported that V, Cr, and Mn partitioned preferentially into the O-rich liquid phase. Extrapolating these data to conditions of the Earth's lower mantle, they suggested that V, Cr, and Mn would have a greater affinity for an O-rich metallic core than for the silicate mantle, due to the increasing solubility of O in molten metal with pressure. Ringwood et al. (1991) reported experiments with V, Cr, and Mn partitioning more strongly into solid silicates rather than solid metal at the lower pressures existing in Mars-sized or smaller bodies. Consequently, they concluded that the material forming the Moon was not from the mantle of a Mars-sized impactor or from the formation of a lunar core. They hypothesized that the V, Cr, and Mn depletions in the Earth and Moon could only have occurred at the ultra-high pressures that exist in the Earth's interior, where the high pressure would cause the formation of an O-rich metallic core, which could deplete the mantle in V, Cr, and Mn. This hypothesis supported the idea that the material forming the Moon originated in the Earth's mantle.

However, additional experimental work by O'Neill et al. (1998) has shown that the solubility of O in liquid metal decreases with increasing pressure, opposite to the behavior suggested by Ringwood et al. (1990, 1991). Also in contrast to the subsolidus partitioning studies of Ringwood et al. (1991), recent models of equilibrium core formation in the Earth have advocated liquid metal–liquid silicate separation in a deep magma ocean. These models have had success in explaining the observed abundances of a number of depleted siderophile elements in the Earth's mantle, such as Ni, Co (Li and Agee, 1996; Li and Agee, 2001a), Mo, P, W (Righter et al., 1997; Righter and Drake, 1999), and even the highly siderophile element Re (Righter and Drake, 1997). Heterogeneous accretion scenarios have also been proposed as an alternative explanation for the abundances of siderophile elements in the mantle (Wänke, 1981; O'Neill, 1991). Unfortunately, such scenarios are more difficult to test directly because they invoke nonequilibrium processes and instead are often indirectly tested by evaluating the success and failure of equilibrium models.

Using metal–magnesiowüstite data as a substitute for direct measurements of metal–silicate partitioning, Gessmann and Rubie (2000) suggested that the depletions of V, Cr, and Mn in the Earth's mantle could similarly be explained by equilibrium core formation in an early magma ocean. Although this model suggests liquid metal–liquid silicate equilibrium, its conclusion is based on experimental liquid metal–magnesiowüstite data and the assumption that there is no significant partitioning difference between liquid silicate and magnesiowüstite for V, Cr, and Mn. The proposed conditions of core formation in the model of Gessmann and Rubie (2000) are more reducing and at a higher temperature and pressure than previous liquid metal–liquid silicate equilibrium core formation models (Li and Agee, 1996; Righter and Drake, 1999). Righter and Drake (2001) claim that at such conditions the depletions of Ni, Co, P, Mo, and W can no longer be explained by equilibrium liquid metal–liquid silicate partitioning. However, recent experimental work suggests the mantle depletions of Ni and Co can indeed be fit by liquid metal–liquid silicate partitioning at conditions similar to those proposed by Gessmann and Rubie (2000) (Li and Agee, 2001a; Chabot and Agee, 2002a).

The most definitive test for core formation in a magma ocean probably comes from partitioning data between liquid metal and liquid silicate. Drake et al. (1989) presented 1 atm experimental data that systematically determined the valence state of V, Cr, and Mn during metal–silicate partitioning. Unfortunately, liquid metal–liquid silicate high-pressure partitioning data for V, Cr, and Mn are limited (Walker et al., 1993; Hillgren et al., 1994; Kilburn and Wood, 1997; Ohtani et al., 1997; Gessmann and Rubie, 1998; Ito et al., 1998; Wade and Wood, 2001). Most experimental work has consisted of a few isolated and scattered experiments, which are useful but often difficult to reconcile and put into context. Metal–silicate partitioning of elements is known to be dependent on a number a thermodynamic variables, such as pressure, temperature, oxygen fugacity, and metallic and silicate compositions. In this study, we present new liquid metal–liquid silicate partitioning data for V, Cr, and Mn that systematically define the effects of these variables. With this improved understanding of the partitioning behavior, we apply the results to core formation, testing the magma ocean hypothesis, as well as discussing implications for the genesis of the Moon. Preliminary results of this work were presented by Chabot and Agee (2000, 2001, 2002b).

2. METHODS

All experiments were conducted at Johnson Space Center in a multi-anvil device using a castable octahedral assembly similar to that of Agee et al. (1995). The starting silicate composition was natural KLB-1 peridotite (Zhang and Herzberg, 1994) or K-feldspar. The mantle peridotite KLB-1 is a commonly used starting material with a relevant planetary composition. The choice of K-feldspar resulted from exploratory experiments and the ability of the silicate to quench to a homogenous glass in the runs (Chabot and Drake, 1999). The two very different starting silicate compositions allowed the effect of the silicate composition on the partitioning behaviors to be examined. The starting metallic composition was a combination of pure, commercially purchased powders of Fe, Ni, FeS, and C. The metallic powders were mixed in varying proportions to determine the effects of S and C on the partition coefficients. Starting mixtures were doped with ~1 wt.% of commercially purchased V, Cr, and Mn oxide powders.

Starting mixtures were contained in MgO, alumina, or graphite capsules. Furnaces of Re foil were used for heating, and a dense alumina sleeve separated the capsule from the furnace. The temperature was monitored by a W3Re/W25Re thermocouple that was positioned perpendicular to the axis of the cylindrical furnace and wrapped around the furnace, as discussed in Agee et al. (1995). Experiments were brought to pressures that ranged between 3 and 14 GPa, as determined from calibrations based on the transitions of quartz to coesite, coesite to stishovite, and forsterite to Mg_2SiO_4 beta phase. All experiments except #V27 were run in castable octahedral assemblies having a truncated edge length (TEL) of 8 mm. The higher pressure of #V27 required an assembly with a 6-mm TEL. Once at pressure, runs were heated to temperatures of 1723 to 2573 K and held for 3 min to 5 h, depending inversely on the temperature. Run durations were based on previous experimental multi-anvil studies of equilibrium partitioning (Thibault and Walter, 1995; Gessmann and Rubie, 1998; Li and Agee, 2001a). Experiments were quenched by suddenly turning off the power to the Re furnace. Run conditions, starting materials, and capsule choices are given in Table 1. Table 1 groups experiments by systematic set in which only one parameter was varied between runs. Some experiments, such as #V3, can belong to multiple sets.

Phase analysis was conducted using the Johnson Space Center Cam-

Table 1. Experimental run conditions and measured metal–silicate partition coefficients.

Run #	Duration (min)	Capsule	Silicate	Metal	T(K)	P(GPa)	X_S	X_C	ΔIW	D(V)	D(Cr)	D(Mn)
v20	5	Alumina	K-spar	Fe	2273	3	0	0	−2.6	0.83 (0.10)	1.06 (0.15)	0.053 (0.013)
v41	5	Alumina	K-spar	Fe, Ni	2273	3	0	0	−2.0	0.41 (0.07)	0.66 (0.11)	0.043 (0.005)
v32	5	Alumina	K-spar	Fe, Ni	2273	3	0	0	−2.2	0.51 (0.04)	0.75 (0.08)	0.053 (0.006)
v21	5	Alumina	K-spar	Fe, FeS	2273	3	0.04	0	−2.4	1.01 (0.08)	1.18 (0.13)	0.061 (0.009)
v30	5	Alumina	K-spar	Fe, FeS	2273	3	0.12	0	−1.9	0.83 (0.35)	1.14 (0.37)	0.052 (0.038)
v9	5	Alumina	K-spar	Fe, FeS	2273	3	0.16	0	−2.1	1.04 (0.20)	1.22 (0.18)	0.065 (0.010)
v22	5	Alumina	K-spar	Fe, FeS	2273	3	0.17	0	−1.6	0.92 (0.22)	1.11 (0.19)	0.081 (0.024)
v25	5	Alumina	K-spar	Fe, FeS	2273	3	0.43	0	−1.4	1.77 (0.29)	3.6 (0.6)	0.75 (0.05)
v31	5	MgO	KLB-1	Fe	2273	3	0	0	−2.9	0.26 (0.05)	1.08 (0.12)	0.15 (0.07)
v49	5	MgO	KLB-1	Fe, FeS	2273	3	0	0	−3.4		2.2 (0.5)	0.21 (0.08)
v44	5	MgO	KLB-1	Fe, FeS	2273	3	0.15	0	−2.5	0.26 (0.11)	1.22 (0.36)	0.19 (0.06)
v3	5	MgO	KLB-1	Fe, FeS	2273	3	0.27	0	−2.2	0.54 (0.14)	1.7 (0.4)	0.26 (0.04)
v45	5	MgO	KLB-1	Fe, FeS	2273	3	0.39	0	−2.0	0.76 (0.54)	2.7 (1.6)	0.85 (0.08)
v34	5	Alumina	K-spar	Fe, C	2273	3	0	0.02	−2.0	0.31 (0.04)	0.60 (0.05)	0.033 (0.008)
v50	5	Alumina	K-spar	Fe, C	2273	3	0	0.13	−2.9	3.7 (0.7)	3.4 (0.6)	0.090 (0.017)
v42	5	Alumina	K-spar	Fe, C	2273	3	0	0.15	−2.4	1.4 (0.8)	1.9 (0.5)	0.11 (0.02)
v11	5	Graphite	K-spar	Fe, FeS, C	2273	3	0.04	0.15	−2.1	1.02 (0.15)	1.67 (0.17)	0.061 (0.022)
v17	5	Graphite	K-spar	Fe, C	2273	3	0	0.17	−2.3	2.9 (0.4)	3.6 (0.27)	0.178 (0.012)
v36	60	Alumina	K-spar	Fe	2123	3	0	0	−2.3	0.39 (0.06)	0.81 (0.13)	0.038 (0.003)
v39	120	Alumina	K-spar	Fe	1973	3	0	0	−2.8	0.59 (0.06)	1.04 (0.23)	0.038 (0.008)
v46	3	Graphite	K-spar	Fe, C	2423	3	0	0.15	−2.9	7.4 (3.5)	6.6 (1.7)	0.18 (0.03)
v47	3	Graphite	K-spar	Fe, C	2573	3	0	0.16	−2.2	3.0 (0.6)	4.3 (1.2)	0.42 (0.05)
v51	255	Alumina	K-spar	Fe, C	1873	3	0	0.08	−3.0	1.08 (0.37)	1.7 (0.7)	0.066 (0.010)
v53	300	Alumina	K-spar	Fe, C	1723	3	0	0.08	−3.2	0.90 (0.39)	1.9 (0.4)	0.025 (0.010)
v54	135	Alumina	K-spar	Fe, C	2073	3	0	0.06	−3.0	1.3 (0.6)	2.2 (0.9)	0.050 (0.012)
v4	5	MgO	KLB-1	Fe, FeS	2273	6	0.24	0	−1.9	0.33 (0.12)	1.1 (0.5)	0.14 (0.03)
v28	5	MgO	KLB-1	Fe, FeS	2273	6	0.25	0	−1.9	0.45 (0.14)	1.6 (0.5)	0.20 (0.05)
v27	5	MgO	KLB-1	Fe, FeS	2273	10	0.24	0	−2.2	0.75 (0.18)	2.2 (0.5)	0.38 (0.07)
v24	5	MgO	KLB-1	Fe, FeS	2273	14	0.24	0	−2.4	0.86 (0.19)	2.4 (0.5)	0.41 (0.08)

Errors in parentheses are $\pm 2\sigma$.

eca SX-100 electron microprobe. Tables 2 and 3 report the compositions of the metallic and silicate liquids. Elements other than V, Cr, and Mn were analyzed using beam conditions of 15 kV and 20 nA and counting times of 20 to 30 s. For the trace elements V, Cr, and Mn, a stronger beam of 15 kV and 100 to 200 nA was used, as well as longer counting times of 30 to 120 s. When S was measured in the silicate, it was also analyzed using the same conditions as those used for V, Cr, and Mn. The O-contents of silicate phases were not measured but instead calculated using the valences of the other elements present.

The C-content of the metallic liquid was also not measured. However, for one microprobe session, all C-bearing runs and run #v20, which is C-free, were carbon coated at the same time. During that session, the metal of all C-bearing runs was analyzed, along with run #V20. The differences in the totals relative to run #V20 were used as the C-contents of the runs. The C-contents determined by this method were roughly consistent with our expected C-contents based on the starting materials used in each run. However, though this method is likely good at determining relative C-contents, the absolute concentration of C is still just an estimate based on the accuracy of the total. We thus estimate our error in the reported C-contents at a similar level to the reported totals, at about ±1 to 1.5 wt.%.

Heterogeneous textures commonly formed during the quenching process, and the analysis was complicated by these quench textures of both the silicate and metallic phases. Figure 1 shows a back-scattered electron (BSE) image of one of the more complicated run products. When the starting silicate was K-feldspar, the silicate quenched to a homogeneous glass. In this case, the glass was examined for compositional gradients but no significant variations were observed, suggesting equilibrium was obtained in the runs. When the starting silicate composition was KLB-1, the silicate, which was a melt at run conditions, did not quench to a single phase but rather formed olivine quench crystals with interstitial glass, as shown in Figure 1b. In the S or C-bearing runs, the quenched metallic liquid was composed of Fe dendrites surrounded by a S-rich or C-rich interstitial phase. Figure 1c shows a BSE image detailing the dendritic texture of a S-bearing metallic phase.

Oxygen-rich exsolution blobs (Fig. 1c) further complicated the analysis of the metallic phase. Similar blobs have been described by O'Neill et al. (1998), who calculated that diffusion over distances up to 100 μm could occur in the metal even during the rapid quenching that takes place in multi-anvil runs. Such diffusion explains the significant blob-free border zone observed in the metal along the boundary with the silicate. This is a serious concern because, along with being O-rich, the blobs also have significant concentrations of V, Cr, and Mn. Thus, to get accurate partition coefficients despite the subsequent alteration of the metal during quenching, large-sized metallic phases were necessary. This was an added challenge, given the already small size of the run products. Care was taken to only measure the metallic phase in regions that would give analyses representative of the composition at run conditions.

Because of these complicating quench textures, multiple measurements with a 50-μm defocused beam were taken to determine the bulk composition of all phases as they were at run conditions. The defocused beam was also a necessity to minimize the volatilization of K and Na during analysis of the silicate glass. Bulk measurements determined on the same run product during different probe sessions were consistent and reproducible, giving confidence in our analytical methods. For the homogenous silicate glass, errors were determined as twice the standard deviation of multiple microprobe measurements. However, for all other phases, differences between individual measurements were due to the quench textures and did not represent how accurately the bulk composition was determined. Twice the standard deviation of the mean was consequently used as the error for measurements of phases with significant quench textures. The lack of appropriate standards complicated the analysis of O in the quenched metallic liquids, and consequently many of the O-contents given in Table 2 are only reported with one significant figure and without errors.

The choice of capsule material affected the resulting run products.

Table 2. Metallic liquid compositions.

Run #	Fe	S	Ni	P	V	Cr	Mn	O	Total
v20	97.9 (0.1)				0.34 (0.03)	0.17 (0.01)	0.010 (0.002)	0.2	98.7
v41	91.3 (0.3)		8.5 (0.1)		0.19 (0.01)	0.125 (0.006)	0.027 (0.002)	0.4	100.5
v32	80.5 (0.2)		18.8 (0.1)		0.27 (0.01)	0.18 (0.01)	0.039 (0.004)	0.4	100.2
v21	95.5 (0.3)	2.3 (0.1)		0.22 (0.01)	0.82 (0.02)	0.33 (0.01)	0.030 (0.004)	0.6	99.8
v30	89.9 (1.3)	7.2 (1.2)		0.54 (0.06)	0.34 (0.14)	0.16 (0.05)	0.025 (0.018)	0.7	98.9
v9	89.8 (0.2)	10.0 (0.2)			0.72 (0.02)	0.28 (0.02)	0.044 (0.0060)	0.5	101.3
v22	85.8 (0.4)	10.6 (0.3)			0.58 (0.13)	0.30 (0.05)	0.054 (0.016)	1.7	99.0
v25	61.4 (0.5)	32.4 (0.4)			1.08 (0.17)	0.76 (0.10)	0.53 (0.02)	3.2	99.4
v31	98.7 (0.3)				0.11 (0.02)	0.226 (0.014)	0.08 (0.04)	0.7	99.8
v49	99.0 (0.3)		n.a.		n.d.	0.061 (0.004)	0.007 (0.002)	0.3	99.4
v44	87.8 (0.7)	9.7 (0.8)	n.a.		0.05 (0.02)	0.11 (0.03)	0.056 (0.016)	2.1	99.8
v3	77.2 (0.7)	18.3 (0.4)	0.45 (0.02)		0.61 (0.13)	0.67 (0.14)	0.25 (0.03)	2.2	99.7
v45	64.3 (0.8)	28.9 (0.6)	n.a.		0.44 (0.29)	0.30 (0.17)	0.51 (0.02)	4.2	98.7
v34	96.3 (0.3)			1.0 (0.1)	0.103 (0.008)	0.078 (0.002)	0.014 (0.003)	0.8	98.3
v50	94.4 (0.1)				0.63 (0.01)	0.37 (0.01)	0.026 (0.004)	0.2	95.6
v42	94.3 (0.2)				0.17 (0.04)	0.15 (0.01)	0.040 (0.006)	0.3	95.0
v11	90.0 (0.4)	2.0 (0.5)			1.32 (0.18)	0.85 (0.08)	0.11 (0.04)	0.6	94.9
v17	92.1 (0.2)				1.0 (0.1)	0.48 (0.02)	0.164 (0.004)	0.7	94.4
v36	100.1 (0.2)				0.11 (0.01)	0.105 (0.002)	0.024 (0.002)	0.3	100.6
v39	99.9 (0.3)				0.071 (0.004)	0.048 (0.002)	0.010 (0.002)	0.3	100.3
v46	92.6 (0.1)			0.33 (0.02)	1.25 (0.02)	0.53 (0.01)	0.054 (0.004)	0.3	95.1
v47	92.7 (0.4)				0.92 (0.03)	0.47 (0.01)	0.21 (0.01)	0.3	94.6
v51	96.2 (0.2)				0.13 (0.01)	0.085 (0.004)	0.019 (0.002)	0.5	96.9
v53	96.0 (0.3)				0.19 (0.01)	0.167 (0.004)	0.007 (0.002)	0.4	96.8
v54	96.7 (0.1)				0.12 (0.01)	0.091 (0.004)	0.012 (0.002)	0.3	97.2
v4	79.8 (0.7)	16.0 (0.7)	0.43 (0.05)		0.63 (0.16)	0.66 (0.15)	0.23 (0.04)	1.2	99.0
v28	80.0 (1.0)	17.4 (0.7)	0.34 (0.03)		0.56 (0.13)	0.60 (0.13)	0.18 (0.04)	2.1	101.2
v27	80.3 (0.5)	16.0 (0.5)	0.37 (0.02)		0.84 (0.20)	0.88 (0.19)	0.27 (0.05)	1.7	100.4
v24	80.9 (0.3)	15.6 (0.2)	0.39 (0.02)		0.67 (0.12)	0.73 (0.13)	0.20 (0.03)	1.4	99.9

n.a. = not analyzed, n.d. = not detected.
Measurements are given as wt%. Errors in parentheses are $\pm 2\sigma$.

Runs conducted in alumina capsules started with the already Al-rich K-feldspar silicate composition, but the final quenched silicate glass was further enriched in Al. Similarly, the final silicate melt composition of experiments that were run in MgO capsules with a starting silicate of KLB-1 was enriched in Mg. Along with affecting the silicate composition, experiments run in MgO capsules frequently produced magnesiowüstite. Table 4 gives the composition of the magnesiowüstite produced in the pressure series experiments, and errors for the magnesiowüstite compositions were calculated as twice the standard deviation of measurements of multiple crystals. Experiments run in MgO capsules with KLB-1 starting material at pressures greater than 3 GPa also contained olivine in the run products. In contrast to alumina and MgO capsules, graphite capsules did not affect the silicate compositions but reacted to form C-rich metallic liquids in the run products.

To test if the higher than natural levels of V, Cr, and Mn in the doped experiments were affecting the partitioning behavior and Henry's law was consequently not obeyed, run #V49, a run with just KLB-1 and Fe metal, was conducted. The silicate KLB-1 is a natural peridotite that is commonly used in studies of the Earth's mantle (Zhang and Herzberg, 1994). Run #V49 is identical to run #V31, except #V31 was doped with V, Cr, and Mn oxides at ~1 wt.%. Vanadium was below detection limits in the undoped run, but the partitioning results for Cr and Mn were consistent between the doped and undoped experiments. Because KLB-1 is a natural and relevant silicate composition, this implies that our experimental results are applicable to natural systems and not affected by the doping of Cr and Mn at wt.% levels, a conclusion that most likely holds for V as well.

3. RESULTS

The liquid metal–liquid silicate weight ratio partition coefficient, D(E), is simply calculated as the weight concentration of element E in the metal divided by the weight concentration of E in the silicate: D(E) = (wt.% E metal)/(wt.% E silicate). Table 1 gives the pressure, temperature, starting compositions, and D(V), D(Cr), and D(Mn) for each experimental run. Tables 2 and 3 give the compositions of the metallic and silicate phases in the quenched run products. Also listed in Table 1 are the calculated atomic concentrations of S (X_S) and C (X_C) in the metallic liquid.

Metal–silicate partition coefficients depend strongly on oxygen fugacity, but unfortunately, in a small, pressurized multi-anvil run, the oxygen fugacity of the experiment is not measured. Instead, we have to rely on estimating the oxygen fugacity during the experiment. The estimated oxygen fugacity is commonly calculated for such experiments relative to the iron–wüstite (IW) buffer, as detailed by Hillgren et al. (1994):

$$\Delta IW = 2 \log (a_{FeO}/a_{Fe}) \quad (1)$$

where a_{FeO} is the activity of FeO in the silicate melt and a_{Fe} is the activity of Fe in the liquid metal. The estimated oxygen fugacity is thus based completely on the partitioning behavior of Fe. If the metal is pure Fe, $a_{Fe} = 1$. However, in the S and C-bearing metallic phases, a_{Fe} was estimated as the atomic concentration of Fe in the metal. The value of a_{FeO} in the silicate was crudely estimated by assuming ideal behavior and using the molar FeO concentration of the quenched silicate as the value of a_{FeO}. The estimated oxygen fugacity for each experiment is listed in Table 1, and the estimates ranged from ~2 to 3 log units below the IW buffer ($\Delta IW = -2$ to -3). In runs that contained magnesiowüstite, ΔIW was also calculated

Table 3. Silicate liquid compositions.

Run #	K	Fe	Na	Si	Ca	Mg	Al	S	V	Cr	Mn	O	Total
v20	8.2 (0.5)	3.9 (0.5)	1.9 (0.1)	23.6 (0.7)			16.6 (0.5)		0.41 (0.03)	0.16 (0.02)	0.19 (0.03)	45.4	100.4
v41	7.2 (0.8)	6.5 (0.8)	1.7 (0.2)	20.1 (1.2)			18.7 (2.2)		0.46 (0.07)	0.19 (0.03)	0.63 (0.06)	43.9	99.4
v32	8.0 (0.3)	4.6 (0.3)	1.8 (0.1)	22.7 (0.3)			16.2 (0.2)		0.53 (0.04)	0.24 (0.02)	0.73 (0.03)	44.4	99.2
v21	8.0 (0.4)	4.1 (0.4)	1.4 (0.1)	20.8 (1.0)			19.2 (0.9)	0.11 (0.07)	0.81 (0.06)	0.28 (0.03)	0.49 (0.03)	44.7	99.9
v30	4.8 (0.1)	7.3 (0.3)	1.4 (0.1)	18.5 (0.6)	0.52 (0.02)	3.7 (0.1)	18.9 (0.4)	0.14 (0.03)	0.41 (0.03)	0.14 (0.01)	0.48 (0.02)	44.5	100.8
v9	8.1 (0.7)	5.4 (1.0)	1.5 (0.1)	22.1 (1.4)			17.6 (0.9)	0.06 (0.02)	0.69 (0.13)	0.23 (0.03)	0.68 (0.04)	45.2	101.5
v22	7.0 (0.3)	8.8 (0.3)	1.3 (0.1)	19.2 (0.4)			18.5 (0.3)	0.13 (0.01)	0.63 (0.05)	0.27 (0.01)	0.67 (0.03)	43.3	99.8
v25	7.3 (0.3)	7.0 (0.4)	1.5 (0.1)	20.8 (0.5)			17.7 (0.5)	0.36 (0.06)	0.61 (0.02)	0.21 (0.02)	0.71 (0.04)	44.0	100.2
v31		3.7 (0.3)		18.1 (0.2)	2.4 (0.4)	28.7 (0.6)	1.4 (0.2)		0.42 (0.04)	0.21 (0.02)	0.55 (0.04)	43.2	98.7
v49		2.4 (0.4)		19.2 (0.4)	1.6 (1.1)	31.7 (1.4)	0.9 (0.5)		n.d.	0.028 (0.006)	0.033 (0.008)	44.9	100.7
v44		4.8 (0.5)		18.1 (0.2)	1.7 (0.4)	29.8 (0.6)	1.3 (0.4)	0.55 (0.12)	0.19 (0.03)	0.09 (0.01)	0.30 (0.04)	43.7	100.5
v3		5.7 (0.5)		17.4 (0.4)	2.4 (0.5)	27.2 (1.2)	2.1 (0.5)	0.39 (0.09)	1.12 (0.16)	0.40 (0.05)	0.96 (0.11)	43.1	100.8
v45		5.5 (0.4)		17.6 (0.4)	2.6 (0.4)	28.3 (0.9)	1.7 (0.4)	0.55 (0.13)	0.58 (0.15)	0.11 (0.02)	0.60 (0.05)	43.3	100.8
v34	5.6 (0.3)	7.0 (0.1)	1.4 (0.1)	18.7 (0.5)	0.42 (0.03)	3.2 (0.1)	18.6 (0.9)		0.33 (0.03)	0.13 (0.01)	0.42 (0.03)	44.1	99.9
v50	8.9 (0.2)	2.3 (0.3)	1.8 (0.1)	26.0 (0.6)			14.0 (0.6)		0.17 (0.03)	0.11 (0.02)	0.29 (0.03)	45.4	99.0
v42	6.9 (0.3)	3.9 (1.1)	1.4 (0.1)	19.8 (0.8)			21.9 (1.0)		0.12 (0.06)	0.08 (0.02)	0.36 (0.04)	45.2	99.7
v11	9.1 (0.5)	5.8 (0.2)	2.1 (0.1)	26.8 (0.3)			9.1 (0.1)	0.06 (0.01)	1.29 (0.05)	0.51 (0.02)	1.81 (0.02)	44.2	100.7
v17	9.8 (0.8)	4.6 (0.4)	2.0 (0.2)	28.0 (0.6)			9.6 (0.1)		0.35 (0.03)	0.132 (0.008)	0.92 (0.06)	44.9	100.3
v36	8.7 (0.2)	5.3 (0.6)	2.0 (0.1)	23.5 (0.8)			14.3 (0.5)		0.28 (0.03)	0.13 (0.02)	0.63 (0.02)	43.8	98.7
v39	9.6 (0.2)	3.0 (0.3)	1.9 (0.1)	26.8 (0.4)			12.1 (0.3)		0.12 (0.01)	0.046 (0.010)	0.26 (0.02)	44.9	98.8
v46	9.2 (0.5)	2.3 (0.2)	2.2 (0.2)	28.6 (0.8)		0.39 (0.08)	10.0 (0.2)		0.17 (0.08)	0.08 (0.02)	0.30 (0.04)	45.2	98.5
v47	9.0 (0.4)	4.9 (1.1)	2.0 (0.1)	26.7 (1.0)		0.43 (0.11)	11.0 (0.5)		0.31 (0.06)	0.11 (0.03)	0.50 (0.06)	44.8	99.7
v51	10.0 (0.4)	2.3 (0.4)	1.9 (0.1)	28.0 (0.6)			11.0 (0.2)		0.12 (0.04)	0.05 (0.02)	0.29 (0.03)	45.2	98.9
v53	8.8 (0.3)	1.9 (0.5)	2.9 (0.1)	29.2 (0.4)			10.1 (0.2)		0.21 (0.09)	0.09 (0.02)	0.28 (0.08)	45.8	99.3
v54	9.6 (0.4)	2.3 (0.2)	2.1 (0.1)	27.6 (0.6)			11.8 (0.2)		0.09 (0.04)	0.042 (0.018)	0.24 (0.04)	45.4	99.2
v4		8.3 (0.9)		15.5 (0.9)	4.8 (1.3)	21.7 (1.9)	3.4 (0.9)	0.25 (0.14)	1.9 (0.5)	0.58 (0.20)	1.6 (0.2)	40.8	98.8
v28		8.0 (1.2)		17.7 (0.5)	4.3 (1.4)	22.4 (2.6)	2.6 (0.6)	0.10 (0.04)	1.25 (0.24)	0.37 (0.07)	0.92 (0.14)	42.2	99.8
v27		6.2 (0.3)		18.4 (0.2)	3.9 (0.2)	23.7 (0.6)	3.2 (0.2)	0.074 (0.012)	1.12 (0.06)	0.40 (0.02)	0.71 (0.03)	43.6	101.3
v24		4.9 (0.3)		19.6 (0.5)	2.9 (0.2)	25.4 (0.9)	2.2 (0.2)	0.11 (0.01)	0.78 (0.10)	0.30 (0.04)	0.49 (0.06)	44.2	100.9

n.d. = not detected.
Measurements are given as wt%. Errors in parentheses are $\pm 2\sigma$.

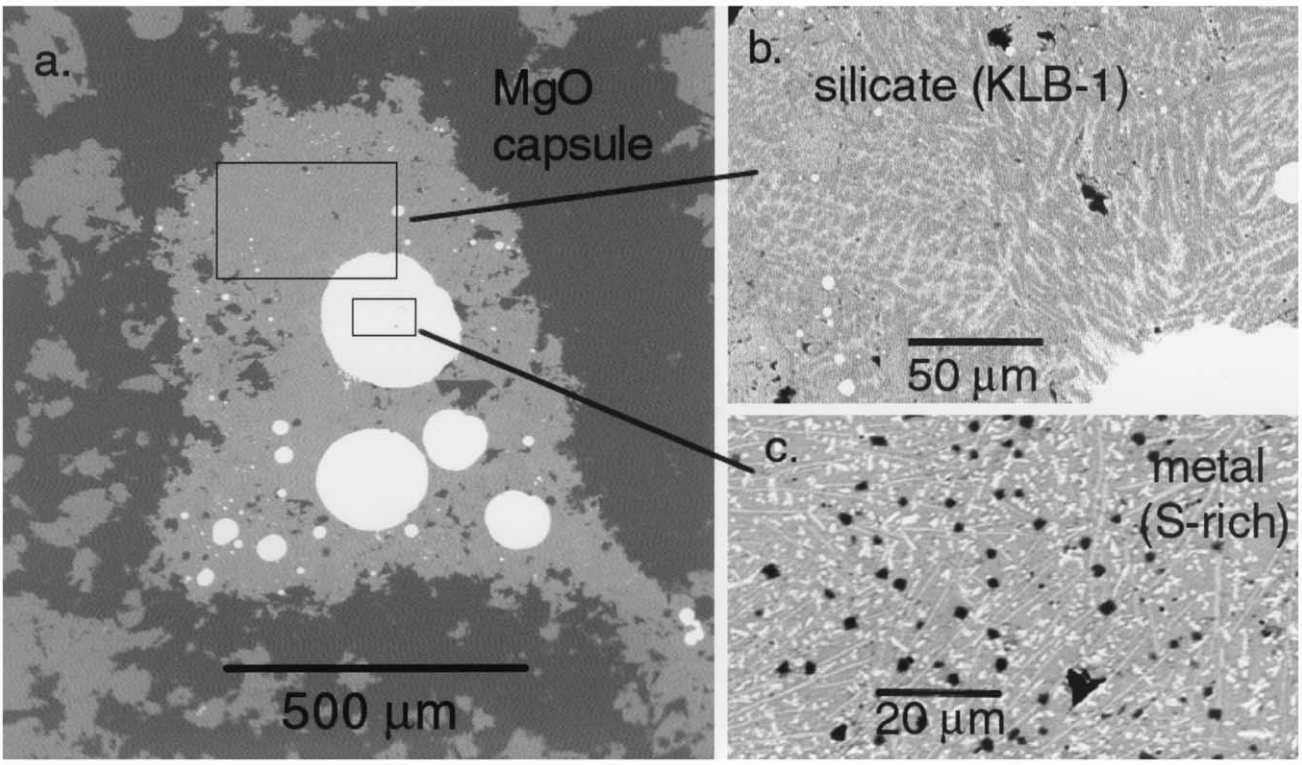

Fig. 1. BSE images of one of the more complicated run products are shown. (a) Metallic and silicate liquids occur as well-separated phases in the run product. The metallic liquid formed discrete blobs, leaving large areas free for analysis of the silicate liquid. (b) Higher resolution imaging of the silicate liquid illustrates the quench texture of olivine crystals with interstitial glass that formed when KLB-1 was used as the starting silicate composition. (c) The metallic liquid exhibited dendritic textures, with Fe dendrites surrounded by FeS in this experiment. Similar dendrites were observed in the C-bearing runs. The small, dark, rounded spots are O-rich phases, not holes in the polished surface. The O-rich phases formed by exsolution during the quenching process.

using the molar FeO content of the magnesiowüstite. Estimating the oxygen fugacity using the magnesiowüstite composition instead of the silicate composition consistently yielded an oxygen fugacity ~0.3 log units higher.

In a systematic set of 1 atm experiments, Drake et al. (1989) found that oxygen fugacity affected the metal–silicate partitioning of V, Cr, and Mn consistent with V being trivalent and Cr and Mn being divalent in the silicate melt. To examine the effects of thermodynamic variables other than oxygen fugacity in our experiments, each run was corrected to an average oxygen fugacity for all the runs of $\Delta IW = -2.4$ using the valences determined in the Drake et al. (1989) study.

To examine the effect of silicate composition, S-bearing experiments conducted at 3 GPa and 2273 K with either K-feldspar or KLB-1 as the starting silicate composition were compared (Fig. 2). Despite the extremely different silicate compositions, the partitioning of both Mn and Cr are similar for the compared experiments, with D(Cr) slightly lower in the experiments that used KLB-1 as the starting silicate composition. On the other hand, D(V) decreases noticeably between runs that used K-feldspar and experiments that started with the more depolymerized KLB-1. Previous experimental studies of other elements (Walter and Thibault, 1995; Jaeger and Drake, 2000) have found metal–silicate partition coefficients commonly decrease with increasing depolymerization of the silicate melt. The larger the valence of the element, the larger was the observed decrease in the previous studies, with divalent elements showing little effect. Thus, the observed effects of sili-

Table 4. Magnesiowüstite compositions.

Run #	Fe	Mg	Al	V	Cr	Mn	O	Total	MW/sil V	MW/sil Cr	MW/sil Mn
v3	7.8 (0.3)	49.5 (0.7)	0.88 (0.07)	3.1 (0.5)	0.65 (0.08)	0.63 (0.05)	37.5	100.0	2.8 (0.6)	1.6 (0.3)	0.66 (0.09)
v4	12.0 (0.5)	40.2 (1.6)	2.7 (0.4)	6.1 (0.9)	1.4 (0.3)	1.08 (0.07)	35.9	99.4	3.2 (1.0)	2.4 (1.0)	0.68 (0.10)
v28	14.8 (1.2)	38.7 (2.0)	3.2 (0.9)	4.7 (1.2)	1.2 (0.3)	0.72 (0.10)	35.4	98.7	3.8 (1.2)	3.2 (1.0)	0.78 (0.16)
v27	10.0 (0.3)	47.5 (0.8)	1.6 (0.1)	2.2 (0.1)	0.56 (0.05)	0.53 (0.02)	36.9	99.3	2.0 (0.2)	1.4 (0.2)	0.75 (0.04)
v24	9.3 (0.6)	48.1 (0.7)	1.2 (0.1)	1.8 (0.1)	0.47 (0.02)	0.47 (0.03)	36.5	97.9	2.3 (0.3)	1.6 (0.2)	0.96 (0.13)

Measurements are given as wt%. Errors in parentheses are $\pm 2\sigma$.

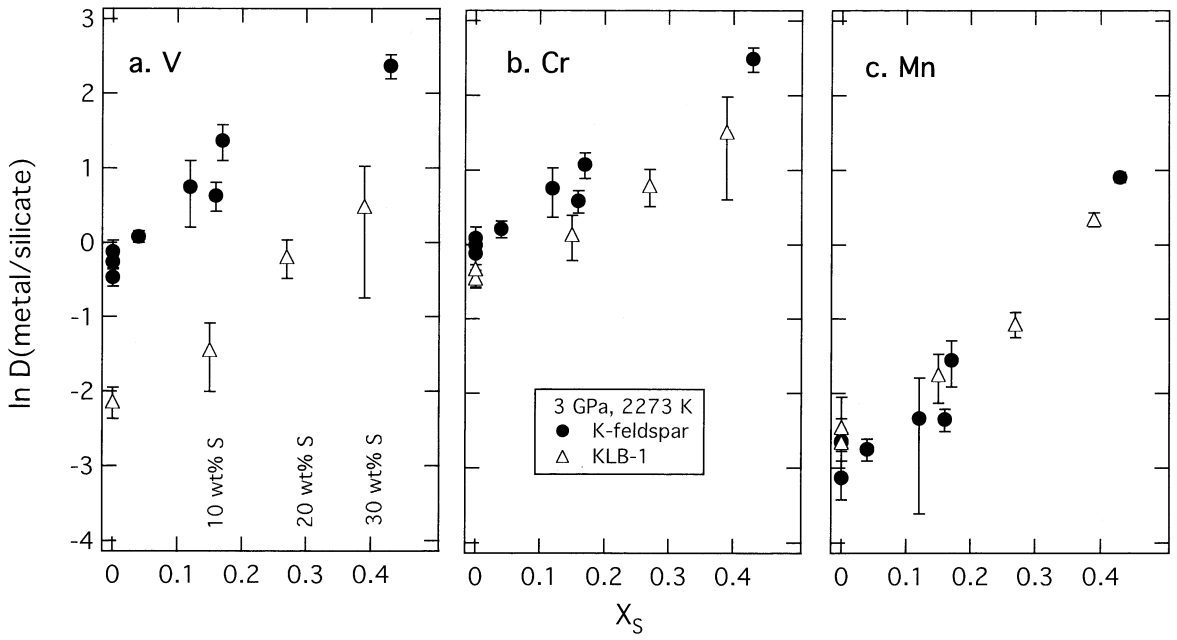

Fig. 2. Metal–silicate partition coefficients for (a) V, (b) Cr, and (c) Mn are plotted against the S-content of the metallic liquid. All results have been corrected to a common oxygen fugacity of –2.4 ΔIW. Two sets of experiments with very different starting silicate compositions, K-feldspar or KLB-1 peridotite, are plotted on each graph. Vanadium partitions preferentially into the more depolymerized KLB-1 melt, as does Cr to a lesser extent. Manganese shows little effect on its partitioning behavior between the two silicate compositions. These results are consistent with V being trivalent and Cr and Mn being divalent. Errors are $\pm 2\sigma$.

cate composition on V, Cr, and Mn are consistent with previous studies and also with the Drake et al. (1989) oxygen fugacity study that found Cr and Mn divalent but V trivalent. The ratios of the partition coefficients between the K-feldspar and KLB-1 experiments were calculated for each element, giving values of 6.4 for V, 1.5 for Cr, and 0.8 for Mn. These ratios were used to compare experiments done with different starting silicate compositions.

The presence of a light element in the metallic liquid can affect the partitioning behavior. Through our experiments, we examined the effects of two elements commonly advocated as possible light elements in planetary cores, S and C (Murthy and Hall, 1970; Wood, 1993; Kilburn and Wood, 1997; Li and Agee, 2001b). Figures 3 and 4 show the effects of S and C on D(V), D(Cr), and D(Mn) at 2273 K and 3 GPa, where the partition coefficients have been corrected to a common ΔIW of –2.4 and silicate composition of K-feldspar, chosen to minimize the number of experiments that needed correcting. All three elements show an increase in D with increasing S-content of the metallic liquid, with the effect being largest for Mn. Similar to the effect of S, increasing the C-content of the metallic liquid also causes D(V), D(Cr), and D(Mn) to increase. Figures 3 and 4 are shown with the same vertical scale for easy comparison. Compared to the effect of S, C in the metallic liquid does not increase the partition coefficients as significantly. This observation is especially true for Mn, which shows about an order of magnitude larger increase in the S-rich system as compared to the C-rich system. It is worth noting that experiments plotted in Figure 4 were run in both alumina and graphite capsules. Despite the different capsule materials and some experiments, consequently, being graphite-saturated, the data form one continuous trend when plotted against the C-content of the metallic liquid. The solid lines in Figures 3 and 4 are second-order, best-fit polynomials to the data that will be used later to parameterize the partition coefficients.

Increasing temperature was found to cause a clear increase in the partition coefficients for all three elements. Figure 5 shows the partitioning behavior of V, Cr, and Mn as a function of temperature from S-free, commonly C-bearing, experiments conducted at 3 GPa and 1723 to 2573 K with a starting silicate composition of K-feldspar. The runs have been corrected to a common ΔIW of –2.4 and X_C of 0.1 using the best-fit polynomials from Figure 4. Manganese, which shows the largest scatter in the data, also shows the largest change in the partitioning behavior with temperature. This significant effect of temperature on D(V), D(Cr), and D(Mn) is similar to that reported for metal–magnesiowüstite partitioning of these elements (Gessmann and Rubie, 1998, 2000). The relationship between ln(D) and 1/T is linear for V, Cr, and Mn, as is expected based on thermodynamic equations.

In contrast to the effect of temperature, the partitioning behavior of V, Cr, and Mn does not vary significantly from 3 to 14 GPa, the pressure range covered in our experiments. Figure 6a shows the data, conducted at 2273 K with S-bearing metal and a starting silicate of KLB-1, corrected to ΔIW of –2.4. Higher pressure data are necessary to establish if any pressure effect does exist. However, our data suggest that the effect of pressure is small, especially in comparison to the effects of temperature shown in Figure 5. Metal–magnesiowüstite parti-

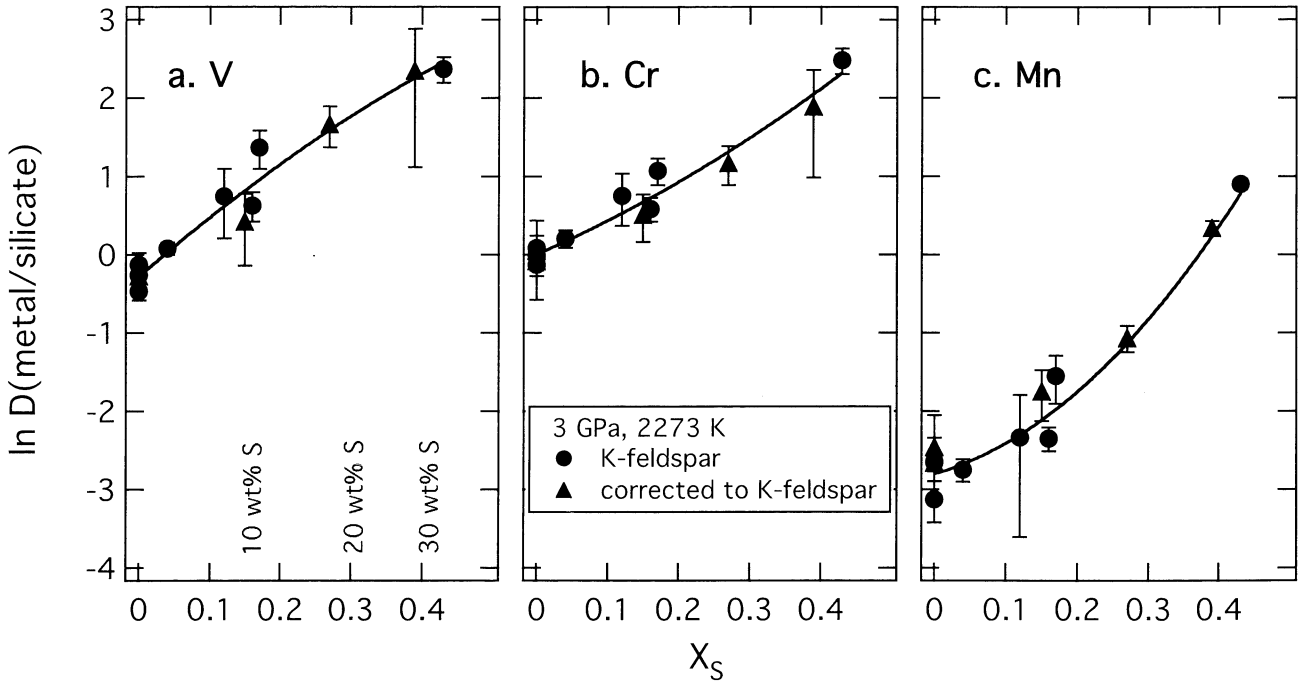

Fig. 3. Experimental metal–silicate partition coefficients for (a) V, (b) Cr, and (c) Mn are plotted against the atomic S concentration of the metallic liquid (X_S) with $\pm 2\sigma$ error bars. For comparison, the experimental data have been corrected to a common oxygen fugacity of –2.4 ΔIW and starting silicate composition of K-feldspar. The presence of S increases the partition coefficients, with the effect being largest for Mn. Solid lines are second-order polynomials fitted to the data and are used in the parameterization of the partition coefficients.

tion coefficients from the same experiments are plotted in Figure 6b, corrected to ΔIW of –2.4 by using the molar FeO-content of the liquid silicate, not the magnesiowüstite, present in each run. The composition of the magnesiowüstite is given in Table 4 and varies between experiments. For example, the two runs at 6 GPa each contain >4 wt.% V and >2 wt.% Al, whereas the concentrations of these elements in the magnesiowüstite of the other experiments are much lower. Compositional effects on the partitioning behavior could explain some of the scatter of Figure 6b. The metal–magnesiowüstite parameterizations given in Gessmann and Rubie (2000) are consistent with our metal–magnesiowüstite data at 2273 K, as plotted on Figure 6b. Because the Gessmann and Rubie (2000) parameterizations used oxygen fugacities estimated from magnesiowüstite instead of silicate melt compositions, a value of ΔIW of –2.1 instead of −2.4 was used to calculate their fits in Figure 6b. Also, our data in Figure 6b are S-bearing but Gessmann and Rubie (2000) did not investigate the effect of S. Consequently, we added our observed effect of S from Figure 3 to the parameterizations of Gessmann and Rubie (2000) so that a comparison could be made.

Despite the scatter in the magnesiowüstite data, some systematic comparisons between metal–magnesiowüstite and metal–silicate partitioning can be drawn. First, the silicate and magnesiowüstite partition coefficients are similar enough that both graphs in Figure 6 can be plotted with the same vertical range. However, for V and Cr, D(metal/silicate) is always larger than D(metal/magnesiowüstite). The compatibility of V and Cr in magnesiowüstite relative to silicate melt could have implications for V and Cr in the lower mantle (Righter, 2003) and is a topic worthy of future studies. For Mn, D(metal/magnesiowüstite) is the larger of the two partition coefficients. Table 4 lists the ratio of magnesiowüstite/silicate for V, Cr, and Mn for further comparison. Also, note the change in the relative order of compatibility from Cr, V, Mn for metal–silicate partitioning to Cr, Mn, V for metal–magnesiowüstite partitioning. Gessmann and Rubie (2000) used metal–magnesiowüstite partitioning data as a substitute for metal–silicate data. Our results indicate that magnesiowüstite is not a perfect proxy for silicate liquid and that direct measurements of D(metal/silicate) should be preferred when examining core formation models.

4. PARAMETERIZING THE DATA

With the effects of pressure, temperature, oxygen fugacity, and metallic and silicate compositions now better understood, the partition coefficient for each element was expressed as a function of these thermodynamic variables:

$$\ln D(V) = [7.9(X_S) - 3.6(X_S)^2] + [-3.7(X_C) + 71(X_C)^2] - 9.7(1000/T) - 3/4(\ln(10))(\Delta IW) - 2.0 \quad (2)$$

$$\ln D(Cr) = [4.0(X_S) + 3.2(X_S)^2] + [-3.4(X_C) + 64(X_C)^2] - 4.4(1000/T) - 2/4(\ln(10))(\Delta IW) - 1.2 \quad (3)$$

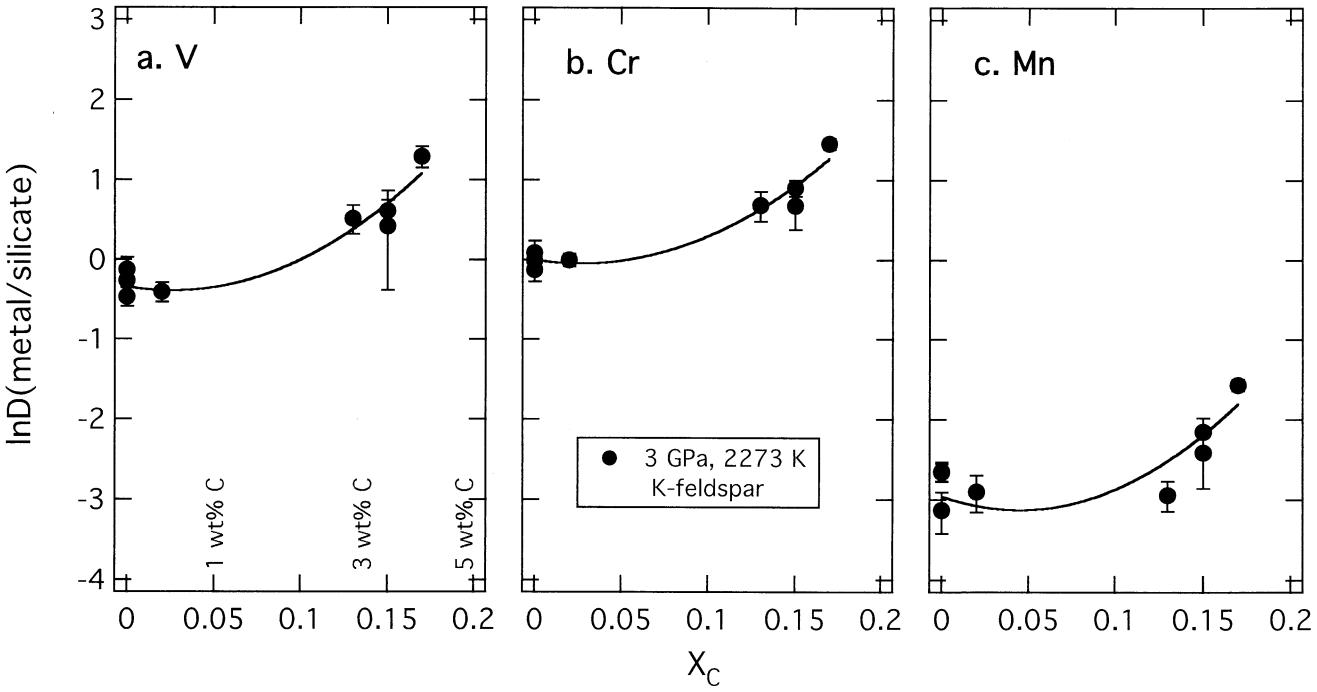

Fig. 4. Metal–silicate partition coefficients for (a) V, (b) Cr, and (c) Mn are plotted against the atomic C-content of the metallic liquid (X_C). Error bars are $\pm 2\sigma$. The presence of C, like S, increases the partition coefficients. Experiments have been corrected to an oxygen fugacity of –2.4 ΔIW. Solid lines are fitted second-order polynomials and are used in the parameterization of the partition coefficients. Experiments were run in both alumina and graphite capsules, yet the data form one continuous trend when plotted against X_C.

$$\ln D(\mathrm{Mn}) = [2.6(X_S) + 13(X_S)^2] + [-7.6(X_C) + 85(X_C)^2] - 11(1000/T) - 2/4(\ln(10))(\Delta \mathrm{IW}) - 0.5 \quad (4)$$

The above parameterizations represent partitioning behavior between liquid metal and liquid silicate with a composition consistent with our experiments that used KLB-1 as the starting silicate material. Because KLB-1 is a naturally occurring mantle peridotite (Zhang and Herzberg, 1994), it is an especially relevant composition to use in models of Earth's core formation. Previous core formation studies (Righter and Drake, 1999; Li and Agee, 2001a) have parameterized the effect of silicate composition by the variable nbo/t (the ratio of nonbridging oxygens over tetrahedral cations in the silicate melt [Mysen, 1991]). However, recent work has shown that nbo/t is an inadequate parameter with which to express the effects of the silicate composition on trace element partitioning behavior, especially for divalent elements (O'Neill and Eggins, 2002). Regardless, for Mn and Cr the silicate composition has little effect on the partitioning behavior, as shown in Figure 2.

The effects of metallic S and C concentrations in Eqns. 2–4 are taken from the curves shown in Figures 3 and 4 for each element. The temperature dependencies in the above parameterizations are from the linear fits in Figure 5. There is no pressure term in the parameterizations, because no pressure effect was observed in the experimental data, as discussed for Figure 6. The effect of oxygen fugacity is expressed using the valences determined by Drake et al. (1989).

The functional form of the parameterizations is generally similar to that used by previous studies (Righter et al., 1997; Righter and Drake, 1997, 1999; Gessmann and Rubie, 2000; Li and Agee, 2001a) to parameterize the partition coefficients for other siderophile elements. One difference is that rather than assuming a functional form for the dependency of D(E) on the metallic composition, such as the form detailed in Jones and Malvin (1990), we chose to fit the experimental data with a polynomial. Because the experiments span the range of interesting S and C contents for planetary core formation, the compositional data will not need to be extrapolated to conditions beyond those of the experiments. Also differing from some previous parameterizations, the oxygen fugacity is represented relative to the IW buffer. The IW buffer will change with temperature and pressure, but because the data were corrected to a common ΔIW before comparisons, the parameterization is self-consistent.

The most significant uncertainties in Eqns. 2–4 are found in the temperature and constant terms. The oxygen fugacity terms are based on the observed valences. The metallic compositions used in this study span the compositions that will be relevant to planetary core formation and consequently will not require extrapolation. In contrast, temperatures much higher than 2573 K, the highest temperature in our experiments, could be reached during the process of planetary core formation. As determined from the best-fit lines on Figure 5, the 1σ uncertainties in the fitted parameters for temperature in Eqns. 2–4 are -9.7 ± 0.9 for V, -4.4 ± 1.0 for Cr, and -11 ± 2 for Mn. Because the value of the constant in Eqns. 2–4 is calculated

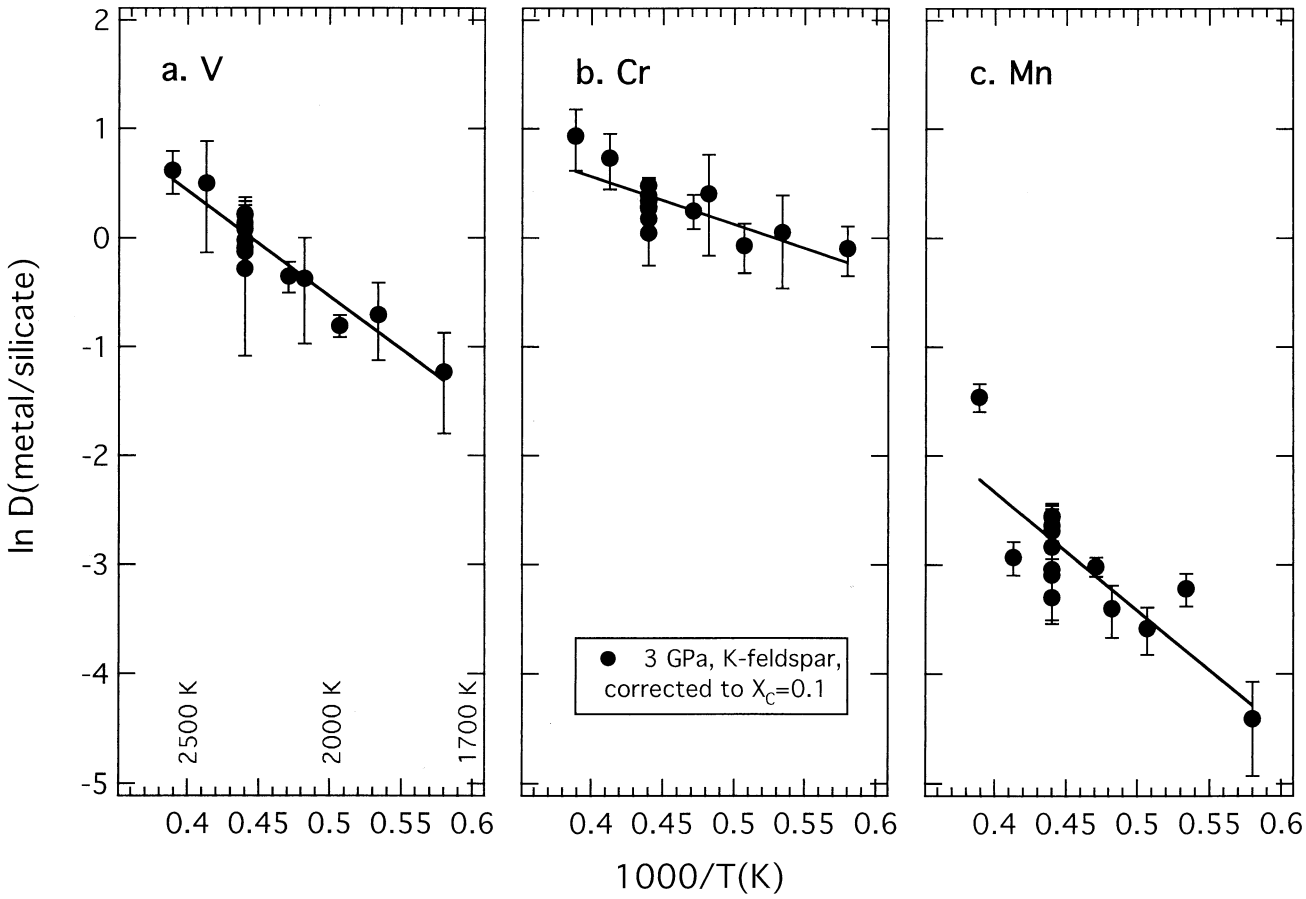

Fig. 5. Experimental metal–silicate partition coefficients for (a) V, (b) Cr, and (c) Mn are plotted as a function of temperature. Experiments were run at 3 GPa with a starting silicate composition of K-feldspar and have been corrected to an average oxygen fugacity of –2.4 ΔIW and X_C of 0.12. The partition coefficients for all three elements increase significantly with increasing temperature. Manganese, which shows the largest scatter in the data, also shows the largest change in the partition coefficient with temperature. The solid lines denote the best-fit line used in the parameterization of the partition coefficients. Experiments are plotted with $\pm 2\sigma$ errors.

after the effect of temperature is parameterized, this uncertainty propagates into uncertainty in the determination of the constant, with values of -2.0 ± 0.4 for V, -1.2 ± 0.4 for Cr, and -0.5 ± 0.9 for Mn.

Using the experimentally determined equations for D(V), D(Cr), and D(Mn), the limited previous liquid metal–liquid silicate data were compared with the values predicted by our parameterizations. To roughly account for the different silicate compositions in previous studies, previous experiments were grouped into one of three categories based on the degree of polymerization of the silicate melt structure: similar to our K-feldspar experiments, similar to our KLB-1 runs, or similar to a 1:1 mix of K-feldspar and KLB-1. The previous experiments were then corrected to a KLB-1 silicate composition using our observed partitioning ratios between K-feldspar and KLB-1 experiments. Though crude, V is the only element of the three really affected by this estimate of the effect of silicate composition, because Cr and Mn show little change in their partitioning behavior with changing silicate composition. Figure 7 plots the comparison between the previous experimental studies and the predicted partitioning values from Eqns. 2–4. Our data from this study are shown as small black dots and show good agreement between measured and predicted partitioning values. This is expected because our data were used to create the parameterizations. However, the large majority of the previous data also falls within a factor of 2 of the predicted values, as shown by the dotted lines in Figure 7. Previous studies are discussed in detail below. The previous data are independent of the parameterization, because they were not used to determine the equations.

As discussed, Drake et al. (1989) conducted a systematic set of 1 atm experiments at 1533 K to examine the effect of oxygen fugacity on the metal–silicate partitioning of V, Cr, and Mn. The results of Drake et al. (1989) are consistent with the earlier abstract of Rammensee et al. (1983) that discussed experiments with variable oxygen fugacities conducted at 1 atm and 1873 K. Due to the lack of metal and silicate compositions listed in the Drake et al. (1989) paper, the oxygen fugacity for each run could not be recomputed by our chosen convention and the values reported in their paper were used instead. The majority of the data from Drake et al. (1989) are fit well by our parameterization (Fig. 7). Any scatter present in the data is not

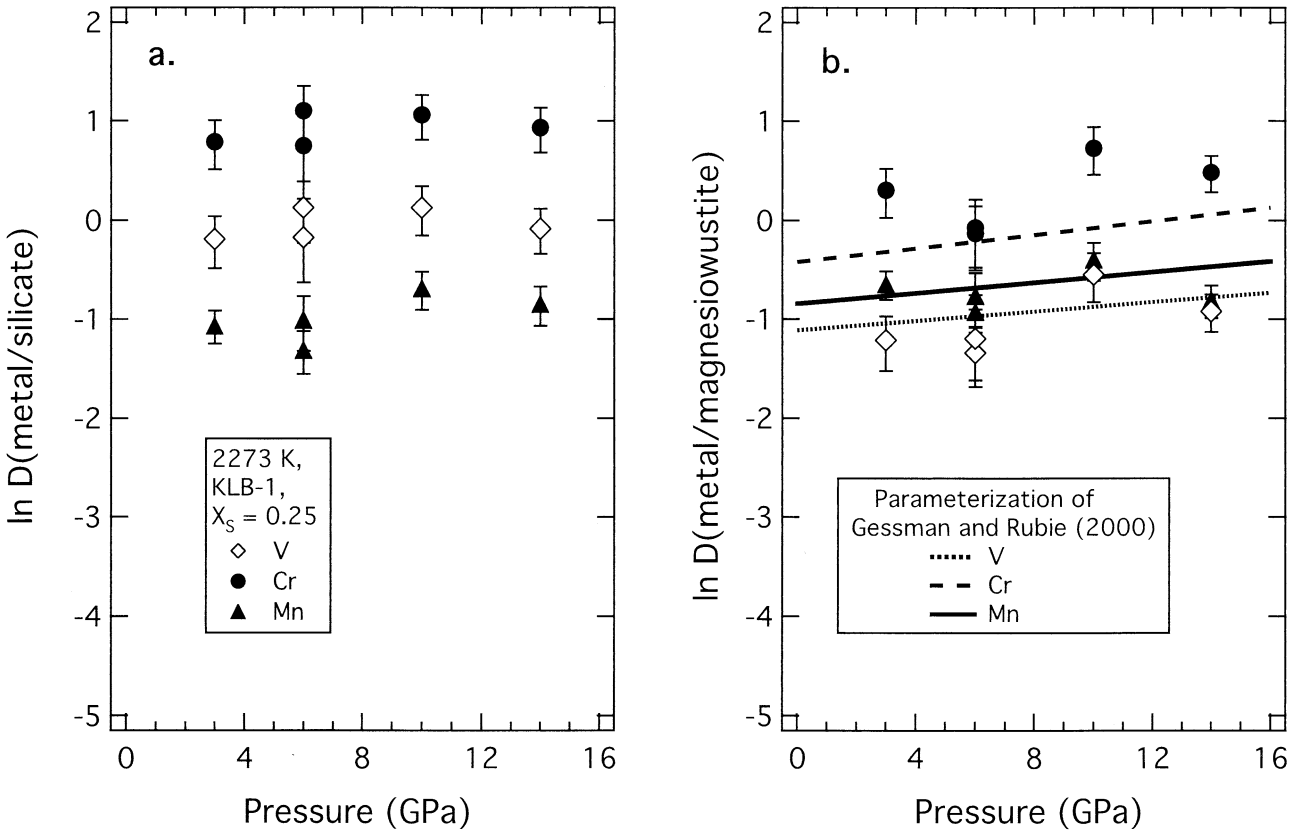

Fig. 6. Partition coefficients for V, Cr, and Mn are plotted for partitioning between (a) liquid metal–liquid silicate and (b) liquid metal–magnesiowüstite. Over the pressure range covered experimentally, the partition coefficients show little variation with pressure. However, differences exist between metal–silicate and metal–magnesiowüstite partitioning, which raises questions about using one as a proxy for the other. Metal–silicate and metal– magnesiowüstite partition coefficients are plotted with $\pm 2\sigma$ errors and have been corrected to a common oxygen fugacity of –2.4 ΔIW, as estimated based on the silicate composition, not the magnesiowüstite composition. Our metal–magnesiowüstite partition coefficients are consistent with the values predicted from the parameterizations given in Gessmann and Rubie (2000).

a reflection on the goodness of our parameterization. The only variable reported in the Drake et al. (1989) work is oxygen fugacity, and the scatter in the data still exists when the data are plotted only against this variable, as shown in their paper. Values for D(Cr) from the Drake et al. (1989) experiments with $\Delta IW < -4$ are not plotted in Figure 7, because they noted that these experiments were not consistent with the rest of their divalent Cr results. The fact that the 1 atm data of Drake et al. (1989) agrees well with our parameterization is further evidence that the effect of pressure is small.

A number of studies have reported a few V, Cr, and Mn experiments conducted at pressures above 1 atm. For consistent comparisons, the oxygen fugacities for all experiments were recomputed using the metal and silicate compositions that they reported and Eqn. 1. Walker et al. (1993) reported two values of D(Cr) at 10 GPa and 2453 and 3073 K. Experiments were conducted in graphite capsules but no C-contents of the metallic liquids were given, though the reported metals were already S-rich. The two experiments of Walker et al. (1993) fall noticeably off our parameterization. However, even in their paper, Walker et al. (1993) noted that the Cr results are anomalous and speculated that Cr contamination may have occurred. In contrast, the results of Hillgren et al. (1994) for V, Cr, and Mn agree exactly with that predicted from our equations. Hillgren et al. (1994) conducted one S-free and C-free experiment at 10 GPa and 2273 K. Kilburn and Wood (1997) reported results for Cr and Mn from four experiments conducted at 2.5 GPa, 2023 K, and oxygen fugacities lower than covered in our study. Despite the much lower oxygen fugacities, which caused significant amounts of Si to be measured in the metallic liquid, the four results from Kilburn and Wood (1997) all fall within a factor of 2 of our predictions.

Two experiments were conducted by Ohtani et al. (1997) at 20 GPa and 2573 and 2773 K, one S-bearing and one S-free. Low totals, La and possibly Cr contamination, and discrepancies between different analytical methods complicated the experiments of Ohtani et al. (1997). Further, the experiments were conducted in graphite capsules but no C-contents were reported. Even with these problems, the reported values of Ohtani et al. (1997) are generally consistent with our parameterization. Gessmann and Rubie (1998) focussed on metal–magnesiowüstite partitioning of V, Cr, and Mn, but in some of their experiments, small amounts of silicate liquid were produced. Despite the difficulty of analyzing small amounts of silicate melt that have a quench texture, for the five runs they reported, run at 9 GPa and 2273 to 2673 K, the values predicted by our param-

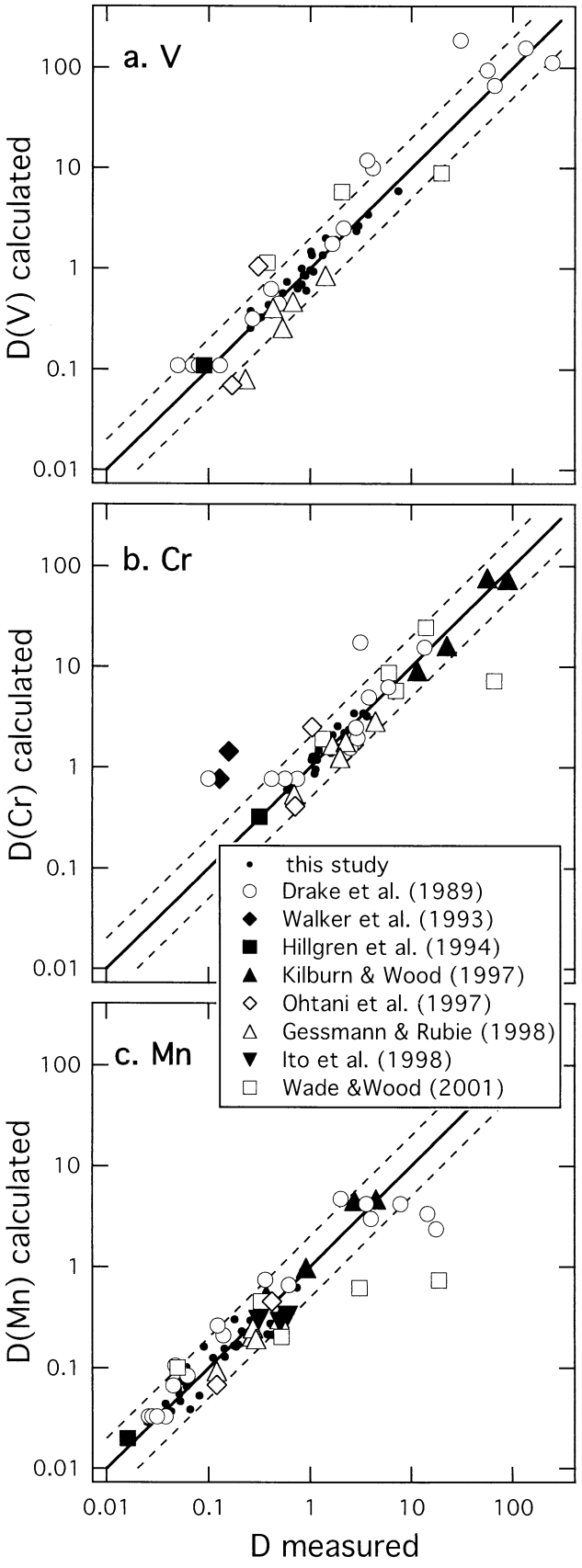

Fig. 7. Previous liquid metal–liquid silicate partitioning data for (a) V, (b) Cr, and (c) Mn are compared to the predicted partition coefficients as calculated from our parameterizations given in Eqns. 2–4. Our data, on which the parameterizations are based, are shown as small black dots. Solid lines are perfect one-to-one agreement. Dotted lines show discrepancies of a factor of 2. The vast majority of the previous experiments fall within a factor of 2 of the parameterized values, despite the wide range of conditions of the previous experiments. The ability of the parameterizations to successfully match the previous results, which were obtained from 1 atm to 25 GPa, without a pressure term, further suggests that pressure has a minor influence on the partitioning behavior.

eterization agree well with their measured partition coefficients. Three S-free and C-free experiments with Mn were conducted by Ito et al. (1998) at 20 to 26 GPa and 2873 K. These experiments suffered from significantly low reported totals for the silicate melt, but the D(Mn) results are matched by our parameterization predictions. Most recently, Wade and Wood (2001) reported two experiments at 2.5 GPa and 2023 K and four runs at 25 GPa and 2573 K. The majority of their runs fall within a factor of 2 of our predicted values. A notable exception is one of their runs that contained 16.4 wt.% Si in the metal and had much higher partition coefficients for all three elements than predicted by our parameterization. We speculate that the high concentration of Si in the metal may have influenced the partitioning behavior.

Overall, the parameterizations of D(V), D(Cr), and D(Mn), based on our systematic experimental results, are able to match the majority of previous liquid metal–liquid silicate partitioning data for these elements. Now, rather than having a disjointed set of two experiments from one study, three experiments at other conditions, etc., all the experimental data for each element can be reconciled in one useful form. The effect of pressure is still lacking in the expressions. However, Eqns. 2–4 successfully matched experiments run from 1 atm to 25 GPa without a pressure term, further suggesting that pressure has a minor influence on the partitioning behavior of these elements.

5. APPLICATION TO CORE FORMATION

With the partition coefficients parameterized, we now examine if the thermodynamic conditions during core formation can explain the Earth's V, Cr, and Mn depletions. Figure 8 illustrates D(V), D(Cr), and D(Mn) calculated from the parameterizations for different core formation conditions. Estimates of the partition coefficients needed to explain the Earth's depletions relative to a chondritic starting composition even after the effects of volatility have been taken into account, as determined in the review chapter of Walter et al. (2000), are also shown in Figure 8.

Righter and Drake (1999) proposed conditions for a magma ocean near 25 GPa, 2250 K, and ΔIW of -0.4, which are similar to some of the conditions advocated in previous studies (Li and Agee, 1996; Righter et al., 1997; Righter and Drake, 1997). For the metallic composition, Righter and Drake (1999) used X_S of 0.1 and X_C of 0.12. At these conditions, V, Cr, and Mn are all incompatible in metal with partition coefficients much less than 1. As shown in Figure 8, raising the temperature, while keeping other variables constant, increases the partition coefficients. However, at ΔIW of -0.4, the partitioning

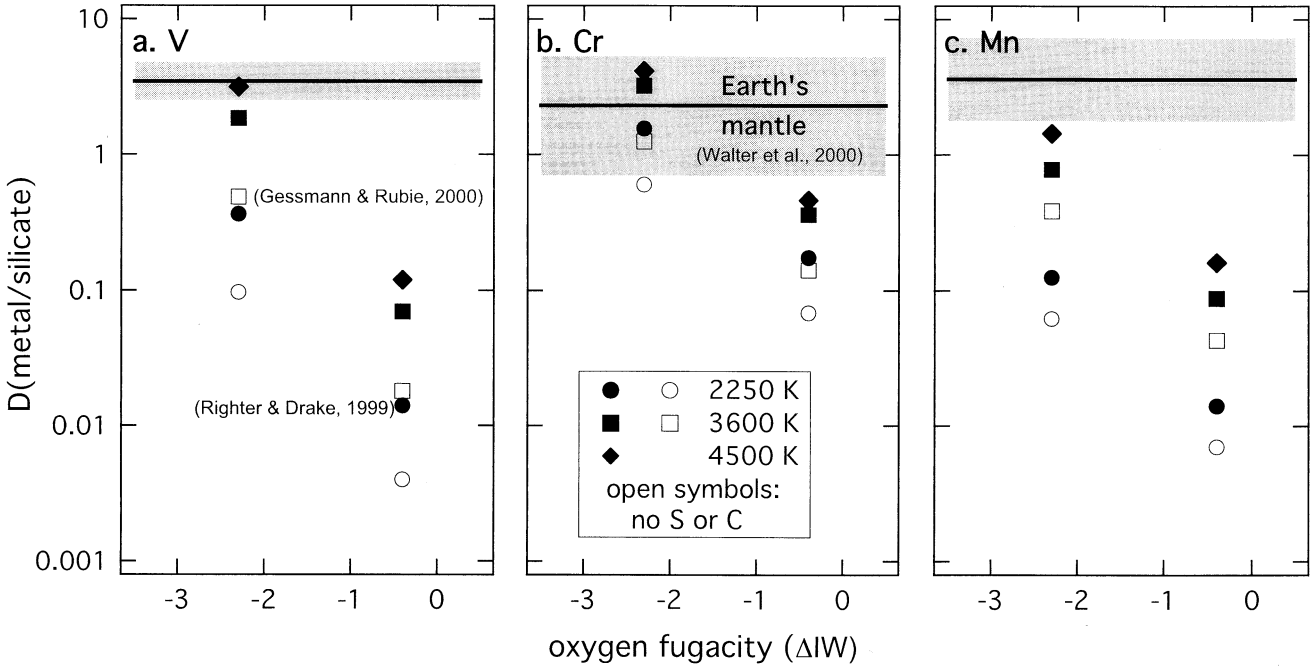

Fig. 8. Calculated partition coefficients for (a) V, (b) Cr, and (c) Mn are plotted against ΔIW to illustrate the effects of different core formation conditions. The partition coefficients needed to explain the mantle depletions in the Earth are shown as black lines, with the shaded regions representing estimates of the uncertainties in the depletions (Walter et al., 2000). All calculations were done using Eqns. 2–4, which are consistent with our experiments that used the mantle peridotite KLB-1 as the starting silicate composition. Solid symbols represent calculations with $X_S = 0.1$ and $X_C = 0.12$; open symbols are S- and C-free. The calculated partition coefficients for V, Cr, and Mn from our parameterizations at the core formation conditions suggested by Righter and Drake (1999) and Gessmann and Rubie (2000) are specifically labeled in the figure. At ΔIW of −0.4, such as the core formation conditions suggested by Righter and Drake (1999), the partition coefficients of all three elements are incompatible in metal, even at 4500 K. However, at a lower oxygen fugacity of ΔIW = −2.3, such as advocated by Gessmann and Rubie (2000), the partition coefficients for V, Cr, and Mn become compatible in metal at high temperatures and can explain the Earth's depletions.

behaviors of all three elements are still incompatible while partition coefficients greater than 1 are necessary to cause any mantle depletions.

The choice of the oxygen fugacity value during core formation significantly influences the partition coefficients applicable to the process. At 3600 K but at more reducing conditions, such as ΔIW of –2.3 instead of −0.4, D(Cr) becomes compatible in metal and D(V) and D(Mn) are also close to being greater than 1. These conditions are similar to those first proposed by Gessmann and Rubie (2000) using metal–magnesiowüstite data as a proxy for metal–silicate partitioning and are also consistent with conditions advocated by Li and Agee (2001a) more recently. In contrast to the work of Righter and Drake (1999), the choice of an oxygen fugacity of –2.3 ΔIW is not from regressing experimental data to match observed mantle depletions of siderophile elements. Instead, it is within the range of calculated oxygen fugacities required for core–mantle equilibrium based on the Earth's present upper mantle with 8 wt.% FeO, an FeNi core with 80 wt.% Fe, and using the method and assumptions, described in Eqn. 1, by which oxygen fugacity is estimated in our experimental runs (Holzheid and Palme, 1996; Li and Agee, 2001a).

Adding some light elements to the metal (Fig. 8) further increases the partition coefficients at 3600 K and −2.3 ΔIW such that D(V) and D(Cr) are both greater than 1 with D(Mn) nearly compatible at a value of 0.78. At yet a higher temperature of 4500 K, all three elements have compatible partition coefficients that fall nearly within the range of acceptable partitioning values to explain the Earth's observed depletions (Walter et al., 2000).

A temperature of 3600 K is a considerable extrapolation of the experimental data, ~1000° higher than the highest run temperature. To what temperatures the observed experimental trends in Figure 5 will hold are unknown. Further, the larger the extrapolation is from the actual experiments, the larger is the uncertainty in the predicted partition coefficient. This is especially an issue for Mn, given the scatter in Figure 5c. A slightly steeper temperature slope through the data in Figure 5c would result in D(Mn) easily falling into the shaded region in Figure 8c as required to explain the Mn depletion in the Earth's mantle. The effect of silicate composition is not accounted for in our parameterizations, which would affect the calculation of D(V) the most. A silicate composition of KLB-1 that was not enriched in Mg, as our experiments were from the MgO capsules, could result in a slightly higher D(V), resulting in D(V) falling into the shaded region in Figure 8a at a slightly lower temperature. The S and C contents used in the calculations for Figure 8 are not unique and could easily have been different without changing the conclusions. The amount of light element is constrained to be ~10 wt.% of the Earth's core (Birch, 1964;

Murthy and Hall, 1970; Wood, 1993), and the identity of the light element in the Earth's core is an actively debated area of research (e.g., review by Hillgren et al., 2000). These data do not indicate what the light element of the core is but do show that if it is a combination of S and C, higher concentrations of V, Cr, and Mn will partition into the core.

Though the data do not indicate a unique set of conditions for core formation, some general conclusions can be drawn. If core formation occurred at a high temperature and a reducing condition near ΔIW of –2.3, the observed depletions of V, Cr, and Mn in the Earth's mantle could be due to a significant amount of these elements partitioning into the metallic core. Although a high-temperature magma ocean at ΔIW near –2.3 may explain the observed mantle depletions of V, Cr, and Mn, high temperatures at more oxidizing conditions, such as ΔIW of −0.4, cannot. These conclusions do not rule out the possibility of lower mantle materials being responsible for the observed depletions (Righter, 2003), but they do show the potential for V, Cr, and Mn to be depleted due to certain core formation conditions. Alternatively, the depletion of Mn in the Earth's mantle may not be due to core formation but due to its volatility. As discussed in the introduction, the Mn/Na ratio in the Earth's mantle is similar to that measured in chondrites, suggesting volatility alone can explain the Mn depletion (O'Neill and Palme, 1998). Unlike Mn, V is refractory and Cr is only slightly volatile. As shown in Figure 8, Mn is the most difficult element of the three to deplete during the model core formation scenarios. If the depletion of Mn can be accounted for by its volatility, the depletions of V and Cr could still be explained by core formation at a high temperature and under reducing conditions.

The experimental data do not provide any direct information regarding the pressure of core formation, but the variables of temperature and pressure are related in a magma ocean scenario if the mantle is partially molten. In this case, the pressure and temperature at the base of the magma ocean will correspond to the intersection of the magma ocean adiabat and the solidus of the mantle material. However, if the mantle is fully molten, the size of the body limits the maximum pressure but not necessarily the maximum temperature of the magma ocean. In other words, both the Earth and a smaller planet could potentially have equally high-temperature magma oceans, but the smaller planet does not possess the higher pressures of the Earth. Thus, the high temperature and ΔIW near –2.3 conditions needed to drive a significant amount of V, and Cr, and possibly Mn, into a metallic core could be achieved in a smaller planetary body than the Earth. A recent estimate of the size of the Moon-forming impactor by Cameron (2000) suggested the impactor was not a small body, having a mass of about a fifth of the mass of the Earth. An alternate study by Canup and Asphaug (2001) advocated a smaller, Mars-sized impactor. The high FeO-content of the present-day Moon may constrain the oxygen fugacity of the material from which it formed, though, as pointed out by Righter (2002), planetary bodies with different FeO contents can be similarly reduced. Overall, with this current understanding, the similarities between the depletions of V, Cr, and Mn relative to chondritic values of the Earth and Moon cannot be used to conclude that the Moon formed from material from the Earth's mantle. This conclusion is compatible with recent dynamical simulations of the Moon-forming impact event that suggest the Moon formed dominantly from material from the impactor, not the Earth's mantle (Cameron, 2000; Canup and Asphaug, 2001).

We conclude that V, Cr, and possibly Mn depletions in the mantles of the Earth and Moon can be explained by core formation in a magma ocean at high temperatures, under low oxygen fugacity (ΔIW ~ –2.3), and in the presence of S and/or C. Because we observe little or no pressure effect on V, Cr, and Mn partitioning in our experiments, we conclude that the mantle depletions of these elements during core formation could occur in planetary bodies with a range of sizes. Accordingly, the V, Cr, and Mn depletions in the lunar mantle could have been derived from a body smaller than the Earth, such as the Moon-forming impactor, if that body had been hot enough and reducing enough during its core formation.

Acknowledgments—This work was supported by NASA grant 344-31-20-25 to C.B.A and NAG5-11122 to R. P. Harvey. N.L.C. held a National Research Council NASA-JSC Research Associateship during the majority of this work. We thank H. St. C. O'Neill, D. C. Rubie, and K. Righter for thorough and thoughtful reviews that significantly improved this manuscript and H. Palme for additional comments and for serving as associate editor.

Associate editor: H. Palme

REFERENCES

Agee C. B., Li J., Shannon M. C., and Circone S. (1995) Pressure-temperature phase diagram for the Allende meteorite. *J. Geophys. Res.* **100,** 17725–17740.

Birch F. (1964) Density and composition of mantle and core. *J. Geophys. Res.* **69,** 4377–4388.

Cameron A. G. W. (2000) Higher-resolution simulations of the giant impact. In *Origin of the Earth and Moon* (eds. R. M. Canup and K. Righter), pp. 133–144. University of Arizona Press, Tucson.

Canup R. M. and Asphaug E. (2001) Origin of the Moon in a giant impact near the end of the Earth's formation. *Nature* **412,** 708–712.

Chabot N. L. and Drake M. J. (1999) Potassium solubility in metal: The effects of composition at 15 kbars and 1900°C on partitioning between iron alloys and silicate melts. *Earth Planet. Sci. Lett.* **172,** 323–335.

Chabot N. L. and Agee C. B. (2000) The effect of core-mantle differentiation on V, Cr, and Mn: Preliminary experimental results. *Proceedings of the Goldschmidt Conference.* **5(2),** Cambridge Publications, 294.

Chabot N. L. and Agee C. B. (2001) The effect of core-mantle differentiation on V, Cr, and Mn: Experimental metal/silicate partitioning results. In *Lunar and Planet. Sci. XXXII*, Abstract #1686, Lunar and Planetary Institute, Houston. (CD-ROM).

Chabot N. L. and Agee C. B. (2002a) The behavior of nickel and cobalt during core formation. In *Lunar and Planet. Sci. XXXIII*, Abstract #1009, Lunar and Planetary Institute, Houston. (CD-ROM).

Chabot N. L. and Agee C. B. (2002b) Core formation in the Earth and Moon: New constraints from V, Cr, and Mn partitioning experiments. *Proceedings of AGU spring meeting*, V51B-09.

Drake M. J., Newsom H. E., and Capobianco C. J. (1989) V, Cr, and Mn in the Earth, Moon, EPB, and SPB and the origin of the Moon: Experimental studies. *Geochim. Cosmochim. Acta* **53,** 2101–2111.

Dreibus G. and Wänke H. (1979) On the chemical composition of the moon and the eucrite parent body and comparison with composition of the Earth: The case of Mn, Cr and V. *Lunar Planet. Sci.* **10,** 315–317.

Gessmann C. K. and Rubie D. C. (1998) The effect of temperature on siderophile element partitioning at 9 GPa and constraints on formation of the Earth's core. *Geochim. Cosmochim. Acta* **62,** 867–882.

Gessmann C. K. and Rubie D. C. (2000) The origin of the depletions of V, Cr, and Mn in the mantles of the Earth and Moon. *Earth Planet. Sci. Lett.* **184,** 95–107.

Hillgren V. J., Drake M. J., and Rubie D. C. (1994) High pressure and high temperature experiments on core-mantle segregation in the accreting Earth. *Science* **264,** 1442–1445.

Hillgren V. J., Gessmann C. K., and Li J. (2000) An experimental perspective on the light element in Earth's core. In *Origin of the Earth and Moon* (eds. R. M. Canup and K. Righter), pp. 245–263. University of Arizona Press, Tucson.

Holzheid A. and Palme H. (1996) The influence of FeO on the solubilities of cobalt and nickel in silicate melts. *Geochim. Cosmochim. Acta* **60,** 1181–1193.

Ito E., Katsura T., and Suzuki T. (1998) Metal/silicate partitioning of Mn, Co, and Ni at high-pressures and high temperatures and implications for core formation in a deep magma ocean. In *Properties of Earth and Planetary Materials at High Pressure and Temperature.* (eds. M. H. Manghnani and T. Yagi), pp. 215–225. *Geophysical Monograph* **101**.

Jaeger W. L. and Drake M. J. (2000) Metal-silicate partitioning of Co, Ga, and W: Dependence on silicate melt composition. *Geochim. Cosmochim. Acta* **64,** 3887–3895.

Jones J. H. and Malvin D. J. (1990) A nonmetal interaction model for the segregation of trace metals during solidification of Fe-Ni-S, Fe-Ni-P, and Fe-Ni-S-P alloys. *Metall. Trans. B* **21B,** 697–706.

Kilburn M. R. and Wood B. J. (1997) Metal-silicate partitioning and the incompatibility of S and Si during core formation. *Earth Planet. Sci. Lett.* **152,** 139–142.

Li J. and Agee C. B. (1996) Geochemistry of mantle-core differentiation at high pressure. *Nature* **381,** 686–689.

Li J. and Agee C. B. (2001a) The effect of pressure, temperature, oxygen fugacity and composition on partitioning of nickel and cobalt between liquid Fe-Ni-S alloy and liquid silicate: Implications for the Earth's core formation. *Geochim. Cosmochim. Acta* **65,** 1821–1832.

Li J. and Agee C. B. (2001b) Element partitioning constraints on the light element composition of the Earth's core. *Geophys. Res. Lett.* **28,** 81–84.

McDonough W. F. (1999) Earth's core. In *Encyclopedia of Geochemistry* (eds. C. P. Marshall and R. W. Fairbridge), pp. 151–156. Kluwer Academic Publishers, Boston.

Murthy V. R. and Hall H. T. (1970) The chemical composition of the Earth's core: Possibility of sulphur in the core. *Phys. Earth Planet. Int.* **2,** 276–282.

Mysen B. O. (1991) Relations between structure, redox equilibria of iron, and properties of magmatic liquids. In *Physical Chemistry of Magmas* (eds. L. L. Perchuk and I. Kushiro), pp. 41–98. Springer, New York.

Ohtani E., Yurimoto H., and Seto S. (1997) Element partitioning between metallic liquid, silicate liquid, and lower-mantle minerals; implications for core formation of the Earth. *Phys. Earth Planet. Int.* **100,** 97–114.

O'Neill H. St. C. (1991) The origin of the Moon and the early history of the Earth—A chemical model. Part 2, The Earth. *Geochim. Cosmochim. Acta* **55,** 1159–1172.

O'Neill H. St. C. and Palme H. (1998) Composition of the silicate Earth: Implications for accretion and core formation. In *The Earth's Mantle, Composition, Structure, and Evolution* (ed. I. Jackson), pp. 3–126. University Press, Cambridge.

O'Neill H. St. C., Canil D., and Rubie D. C. (1998) Oxide-metal equilibria to 2500°C and 25 GPa: Implications for core formation and the light component in the Earth's core. *J. Geophys. Res.* **103,** 12239–12260.

O'Neill H. St. C., and Eggins S. M. (2002) The effect of melt composition on trace element partitioning: An experimental investigation of the activity coefficients of FeO, NiO, CoO, MoO_2 and MoO_3 in silicate melts. *Chem. Geol.* **186,** 151–181.

Rammensee W., Palme H., and Wänke H. (1983) Experimental investigation of metal-silicate partitioning of some lithophile elements (Ta, Mn, V, Cr). *Lunar Planet. Sci.* **XIV,** 628–629.

Righter K., Drake M. J., and Yaxley G. (1997) Prediction of siderophile element metal/silicate partition coefficients to 20 GPa and 2800°C: The effects of pressure, temperature, oxygen fugacity and silicate and metallic melt compositions. *Phys. Earth Planet. Int.* **100,** 115–134.

Righter K. and Drake M. J. (1997) Metal-silicate equilibrium in a homogeneously accreting earth: New results for Re. *Earth Planet. Sci. Lett.* **146,** 541–553.

Righter K. and Drake M. J. (1999) Effect of water on metal-silicate partitioning of siderophile elements: A high pressure and temperature terrestrial magma ocean and core formation. *Earth Planet. Sci. Lett.* **171,** 383–399.

Righter K. and Drake M. J. (2001) Constraints on the depth of an early terrestrial magma ocean. *Meteorit. Planet. Sci.* **36,** A.173.

Righter K. (2002) Does the Moon have a metallic core? Constraints from giant impact modeling and siderophile elements. *Icarus* **158,** 1–13.

Righter K. (2003) Partition coefficients at high pressure and temperature. In *Treatise on Geochemistry*, Volume 2: Geochemistry of the Mantle and Core (ed. R.W. Carlson), in press.

Ringwood A. E. (1986) Terrestrial origin of the Moon. *Nature* **322,** 323–328.

Ringwood A. E. (1966) The chemical composition and origin of the Earth. In *Advances in Earth Science* (ed. P. Hurley), pp. 357–398. MIT Press, Boston.

Ringwood A. E., Kato T., Hibberson W., and Ware N. (1991) Partitioning of Cr, V and Mn between mantles and cores of differentiated planetesimals: Implications for giant impact hypothesis of lunar origin. *Icarus* **89,** 122–128.

Ringwood A. E., Kato T., Hibberson W., and Ware N. (1990) High pressure geochemistry of Cr, V and Mn and implications for the origin of the Moon. *Nature* **347,** 174–176.

Thibault Y. and Walter M. J. (1995) The influence of pressure and temperature on the metal-silicate partition coefficients of nickel and cobalt in a model C1 chondrite and implications for metal segregation in a deep magma ocean. *Geochim. Cosmochim. Acta* **59,** 991–1002.

Wade J. and Wood B. J. (2001) The Earth's 'missing' niobium may be in the core. *Nature* **409,** 75–78.

Walker D., Norby L., and Jones J. H. (1993) Superheating effects on metal-silicate partitioning of siderophile elements. *Science* **262,** 1858–1861.

Walter M. J. and Thibault Y. (1995) Partitioning of tungsten and molybdenum between metallic liquid and silicate melt. *Science* **270,** 1186–1189.

Walter M. J., Newsom H. E., Ertel W., and Holzheid A. (2000) Siderophile elements in the Earth and Moon: Metal/silicate partitioning and implications for core formation. In *Origin of the Earth and Moon* (eds. R. M. Canup and K. Righter), pp. 265–289. University of Arizona Press, Tucson.

Wänke H. (1981) Constitution of terrestrial planets. *Phil. Trans. R. Soc. Lond. A* **303,** 287–302.

Wänke H. and Dreibus G. (1986) Geochemical evidence for the formation of the Moon by impact-induced fission of the proto-Earth. In *Origin of the Moon* (eds. W. K. Hartmann, R. J. Phillips, and G. J. Taylor), pp. 649–672. Lunar and Planetary Institute, Houston.

Wood B. J. (1993) Carbon in the core. *Earth Planet. Sci. Lett.* **117,** 593–607.

Zhang J. and Herzberg C. (1994) Melting experiments on anhydrous peridotite KLB-1 from 5.0 to 22.5 GPa. *J. Geophys. Res.* **99,** 17729–17742.